

Optical characterization of dyed liquid crystal cells

Obeng Appiagyei Addai^{1*}, Ruilin Xiao^{2†}, Xiaoyu Zheng^{1 ‡}, Peter Palffy-Muhoray^{1,2§}

¹*Department of Mathematical Sciences, Kent State University, OH, USA*

²*Advanced Materials and Liquid Crystal Institute, Kent State University, OH, USA*

August 31, 2022

Abstract

The guest-host liquid crystal display, first proposed in 1968, relies on controlling the orientation of dichroic dyes dissolved in a nematic liquid crystal host. Controlling the orientation of the liquid crystal and of the dissolved dye with an electric field allows control of the transmittance of the cell. Knowing the dielectric properties at optical frequencies of the dye and liquid crystal mixtures is crucial for the optimal design of guest-host liquid crystal devices. In this work, the dielectric functions of various layers in liquid crystal cells are described by models obeying the Kramers-Kronig relations: the Sellmeier equation for transparent layers and causal Gaussian oscillator model for absorbing layers. We propose a systematic way to accurately model the dielectric response of each layer by minimizing the sum of squared differences between the measured transmittance spectrum of a guest-host cell in the near-UV/vis range and the prediction of the transmittance of the modeled multilayer structure. By measuring the transmittance for incident light polarized parallel and perpendicular to the nematic director allows us to separately characterize the two principal dielectric functions of the uniaxial sample. Our results show that the causal Gaussian oscillator model can accurately characterize the dielectric functions of dyes in liquid crystals.

keywords: dielectric functions, dichroic dyes, guest-host liquid crystals, causal Gaussian oscillator model

1 Introduction

Dyes are colored since their absorption is wavelength dependent. They have a wide range of applications, including information displays, such as LCDs. The first guest-host liquid crystal display was proposed by Heilmeyer and Zanoni in 1968 [1], where dichroic dyes are dissolved in nematic liquid crystals (NLCs). The transmittance of the NLC cell is controlled by an electric field which can orient the LC molecules, which in turn orient the dichroic dye molecules. The optical response depends on polarizabilities of the constituents, hence their dielectric tensors at optical frequencies. Many guest-host liquid crystal systems have been subsequently proposed and realized; various aspects of these systems have been studied and reported, as in early review papers by Cox in 1979 [2] and by Scheffer in 1983 [3], and more recently by Sims in 2016 [4].

Modeling the dielectric function of dyes in LCs at optical frequencies can be a powerful tool for the interpretation of measured transmittance spectra and for predicting the transmittance and reflectance as function of wavelength. Characterization of the dielectric function of dyes in solutions is a challenging task in general, as dyes molecules often show the tendency to associate causing the transmittance to depend nonlinearly on concentration and absorption peaks to shift when mixing two dyes [5]. However, at low concentrations, one can assume the linear response.

An overview of most popular models for dielectric functions and their applicabilities can be found in [6]. Among those models, the classical Lorentz model assumes that the motion of the electrons, bound to atomic

*Email: oaddai@kent.edu, ORCID 0000-0003-0024-7989

†Email: rxiao@kent.edu, ORCID 0000-0001-9001-098X

‡Corresponding author, Email: xzheng3@kent.edu, ORCID 0000-0002-3787-7741

§Email: mpalffy@kent.edu, ORCID 0000-0002-9685-5489

nuclei, can be modeled as a simple damped harmonic oscillator, subject to the external electromagnetic fields. The dielectric function ε can then be expressed as (e.g. [7])

$$\varepsilon^{LO}(\omega) = \varepsilon_\infty + \sum_{k=1}^N \frac{A_k \omega_p^2}{\omega_{0k}^2 - \omega^2 - i\gamma_k \omega}, \quad (1.1)$$

where ε_∞ is the high frequency dielectric constant, ω_p is the plasma frequency, A_k is the strength of the k th oscillator with resonant frequency ω_{0k} and the damping coefficient γ_k . The damping coefficient γ_k is proportional to the width of the absorption peak. Taking the limit of $\gamma_k \rightarrow 0$ in Eq. (1.1) gives the Sellmeier equation,

$$\varepsilon^S(\omega) = \varepsilon_\infty + \sum_{k=1}^N \frac{A_k \omega_p^2}{\omega_{0k}^2 - \omega^2}, \quad (1.2)$$

which is often used to model the dispersion relations for transparent materials away from the absorption peaks. The Lorentz oscillator model satisfies the Kramers-Kronig (KK) causality relations. Some authors [8, 9] have used Lorentz oscillator models for dispersion relations for azo-dyes. The Lorentz oscillator model can produce realistic absorption frequencies and amplitudes. However, as the Lorentz oscillator model tends to predict slower decays, the fitting to the absorption data is poor away from the absorbance peaks [9, 10].

In 1992, Brendel and Bormann (BB) proposed a dielectric function model for amorphous solids in the infrared (IR) range [11]. It is written as a convolution of a Gaussian function with the Lorentz oscillator

$$\varepsilon^{BB}(\omega) = \varepsilon_\infty + \sum_{k=1}^N \chi_k^{BB}(\omega), \quad (1.3)$$

where

$$\chi_k^{BB}(\omega) = \frac{1}{\sqrt{2\pi}\sigma_k} \int_{-\infty}^{\infty} \exp\left(-\frac{(x - \omega_{0k})^2}{2\sigma_k^2}\right) \frac{A_k \omega_p^2}{(x^2 - \omega^2) - i\omega\gamma_k} dx. \quad (1.4)$$

It was interpreted as the superposition of damped harmonic oscillators whose resonance frequencies follow a Gaussian distribution centered at ω_{0k} with standard deviation σ_k . Some authors [10, 12, 13] used the Brendel and Bormann model, sometimes referred to as Voigt model, for modeling the dielectric functions of dyes and showed improved accuracy over the Lorentz oscillators. Subsequently it was shown that the BB model is not causal as it fails to satisfy $\chi_k^{BB}(\omega) \neq \overline{\chi_k^{BB}(-\omega)}$ in addition to a divergent behavior near $\omega = 0$ [14].

Meneses *et. al.* [15] in 2006 proposed the causal Gaussian oscillator model, to model the dielectric function of binary lead silicate glasses,

$$\varepsilon^{CG}(\omega) = \varepsilon_\infty + \sum_{k=1}^N \chi_k^{CG}(\omega), \quad (1.5)$$

where the imaginary part of χ_k^{CG} is given by

$$\chi_k^{CG''}(\omega) = A_k \left[\exp\left(-\frac{(\omega - \omega_{0k})^2}{2\sigma_k^2}\right) - \exp\left(-\frac{(\omega + \omega_{0k})^2}{2\sigma_k^2}\right) \right], \quad (1.6)$$

and the real part, which guarantees satisfying the KK relations, is given in terms of the Dawson function $D(x)$ as

$$\chi_k^{CG'}(\omega) = \frac{2A_k}{\sqrt{\pi}} \left[D\left(\frac{\omega + \omega_{0k}}{\sqrt{2}\sigma_k}\right) - D\left(\frac{\omega - \omega_{0k}}{\sqrt{2}\sigma_k}\right) \right], \quad (1.7)$$

where $D(x) = e^{-x^2} \int_0^x e^{t^2} dt$. The causal Gaussian oscillator model can be obtained by removing the divergent factor from the BB oscillator model and setting $\gamma_k = 0$. It has been used to characterize silica glass in the far IR region [16], and Titanium dioxide from near-UV to near-IR [17].

We point out that in Ref. [18], the authors used the renormalized ellipsometry to determine the device parameters and tilt angles of a guest-host LC system. In particular, they have used a combined Cauchy

equation and Gaussian model for the complex refractive indices of a guest-host LC system. Their assumed dielectric function does not obey the KK relations. Nonetheless, they showed that the extinction coefficient of the guest-host LC system can be characterized by a Gaussian function.

In another vein, calculations based on density functional theory or molecular dynamics were carried out to predict the polarizabilities of dyes [10] and the alignment of dyes in LCs [19, 20]. These calculations require knowledge of the specific molecular structures to find the minimum potentials and their frequency dependence.

In this work, the characterization of the dielectric functions of our samples is solely based on the transmittance spectra, without the knowledge of their molecular structures. Specifically, we model the dielectric function of each layer in our multilayer LC samples in the near-UV/vis range by either the Sellmeier equation, if they appear transparent or by the causal Gaussian oscillator model, if they have absorption. We show that the dielectric function of the dye and liquid crystal mixture can be accurately described by the causal Gaussian oscillator model.

The rest of the paper is organized as follows. In section 2, we present the mathematical models and methods which lead to the determination of the parameters in the dielectric function models. Section 3 describes our experimental setup for obtaining the transmittance spectra of our samples. In section 4, we show the characterization results of dielectric functions of all components in our guest-host LC sample. We give our conclusions in section 5.

2 Mathematical Models and Methods

In this section, we first briefly discuss the eigenvalue problem associated with light propagation in a lossy uniaxial material, explain the setup of our experiments and discuss the validity of applying the averaged transmittance model of a multilayer structure to our problem. Then we present the least squares approach used to determine the parameters in the dielectric function models where we minimize the sum of the squared differences between the experimental measurements and the results of theoretical models.

A uniform uniaxial material is birefringent, and the polarization of plane polarized light will, in general, change as it propagates through the material unless the polarization is along one of two eigen directions associated with the wave propagation direction. The eigenvalue problem in term of the displacement field \mathbf{D} , derived from Maxwell equation, is given by (cf. [7])

$$(k^2 \mathbf{I} - \mathbf{k}\mathbf{k})\varepsilon_r^{-1} \mathbf{D} = k_0^2 \mathbf{D}, \quad (2.1)$$

where \mathbf{I} is the identity tensor, $\mathbf{k} = k'\hat{\mathbf{k}}' + ik''\hat{\mathbf{k}}''$ is the complex wave vector, $k^2 = \mathbf{k} \cdot \mathbf{k} = k'^2 - k''^2 + 2ik'k''(\hat{\mathbf{k}}' \cdot \hat{\mathbf{k}}'')$ is the dot product, $\mathbf{k}\mathbf{k}$ is the tensor product, and $k_0^2 = \omega^2 \mu_0 \varepsilon_0$, where μ_0 is the permeability, ε_0 is permittivity of free space, and ω is the angular frequency. For uniaxial absorbing materials, the complex relative dielectric tensor can be written as

$$\varepsilon_r = \varepsilon_{\perp} \mathbf{I} + (\varepsilon_{\parallel} - \varepsilon_{\perp}) \hat{\mathbf{n}}\hat{\mathbf{n}}, \quad (2.2)$$

where ε_{\parallel} is the dielectric constant for fields parallel to the symmetry axis $\hat{\mathbf{n}}$, and ε_{\perp} is the dielectric constant for fields in the plane perpendicular to $\hat{\mathbf{n}}$. In our LC samples, the symmetry axis $\hat{\mathbf{n}}$ coincides with the director of the nematic liquid crystal.

Given the directions of $\hat{\mathbf{k}}'$ and $\hat{\mathbf{k}}''$ and ε_r , one can solve for the eigenvalues k' , k'' , and for the corresponding eigenvector \mathbf{D} . One eigen-pair is given by

$$k_1^2 = k_0^2 \varepsilon_{\perp}, \mathbf{D}_1 \parallel \hat{\mathbf{n}} \times \mathbf{k}_1, \quad (2.3)$$

while the other is given, implicitly, by

$$k_2^2 \varepsilon_{\perp} + \Delta \varepsilon (\hat{\mathbf{n}} \cdot \mathbf{k}_2)^2 = k_0^2 \varepsilon_{\parallel} \varepsilon_{\perp}, \quad (2.4)$$

and

$$\mathbf{D}_2 \parallel \mathbf{k}_2 \times (\hat{\mathbf{n}} \times \mathbf{k}_2). \quad (2.5)$$

Similar results can be found in [21].

Suppose light propagating in an isotropic lossless medium is normally incident on a nematic LC cell where the director $\hat{\mathbf{n}}$ is along the $\hat{\mathbf{x}}$ direction. Boundary conditions require that, in the cell, $\hat{\mathbf{k}} = \hat{\mathbf{k}}' = \hat{\mathbf{k}}'' = \hat{\mathbf{z}}$. If the polarization of plane polarized incident light, and hence the direction $\hat{\mathbf{E}}$ of the electric field of the incident light is perpendicular to $\hat{\mathbf{n}}$, we have, by Eq. (2.3),

$$k_1^2 = k_0^2 \varepsilon_{\perp}, \mathbf{D}_1 \parallel \mathbf{E}_1 \parallel \hat{\mathbf{y}}. \quad (2.6)$$

That is, the polarization of the light will remain in the $\hat{\mathbf{y}}$ -direction, and the wave number in the sample is only dependent on ε_{\perp} . If the linear polarization is such that $\hat{\mathbf{E}}$ is parallel to $\hat{\mathbf{n}}$, we obtain from Eqs. (2.4)-(2.5),

$$k_2^2 = k_0^2 \varepsilon_{\parallel}, \mathbf{D}_2 \parallel \mathbf{E}_2 \parallel \hat{\mathbf{x}}. \quad (2.7)$$

That is, the polarization of the light will remain in the $\hat{\mathbf{x}}$ -direction, and the wave number in the sample is only dependent on ε_{\parallel} . Those correspond to the two cases depicted in Fig. 1, and indicate the geometries considered in this work.

In these two scenarios, we can then use the following recursive relations to calculate the transmission and reflection coefficients for light propagation through an isotropic multilayer structure at normal incidence, with light incident from medium 1 and exiting to medium m (see, e.g. [22]),

$$t_{1:m} = \frac{t_{12} t_{2:m} e^{ik_0 n_2 d_2}}{1 + r_{12} r_{2:m} e^{2ik_0 n_2 d_2}}, \quad (2.8)$$

$$r_{1:m} = \frac{r_{12} + r_{2:m} e^{2ik_0 n_2 d_2}}{1 + r_{12} r_{2:m} e^{2ik_0 n_2 d_2}}, \quad (2.9)$$

where

$$r_{ij} = \frac{n_i - n_j}{n_i + n_j}, t_{ij} = \frac{2n_i}{n_i + n_j}, \quad (2.10)$$

$$n_i = \sqrt{\varepsilon_i}, i = 1, \dots, m. \quad (2.11)$$

Here n_i is the complex refractive index whose real and imaginary parts are referred to as the index of refraction and the extinction coefficient, respectively. The transmittance and reflectance of the multilayer structure, with $n_1 = n_m$, can be readily obtained from

$$T_{1:m} = |t_{1:m}|^2, R_{1:m} = |r_{1:m}|^2. \quad (2.12)$$

A general result for transmittance and reflectance of anisotropic absorbing multilayer structure can be found in [23]. We note that a decrease in the transmittance of a multilayer structure can be due to absorption in the layers and/or to reflections at the interfaces. In the case of absorption, the refractive index has a nonzero imaginary part, originating in the imaginary part of ε , and in the case of reflections, there is a mismatch of the refractive indices of adjacent layers.

The transmittance and reflectance from Eq. (2.12) of a thick ($d \gg \lambda$) single- or multilayer structure can show large and rapid oscillations as function wavelength due to interference and multiple reflections. These become increasingly difficult to observe experimentally as the sample thickness increases, due to the finite resolution of spectrometers and sample inhomogeneities. In this limit, ignoring multireflection interference, or, equivalently, by assuming random phase, the average transmittance $\mathcal{T}_{1:m}$ and reflectance $\mathcal{R}_{1:m}$ for a multilayer structure at normal incidence are given by

$$\mathcal{T}_{1:m} = \frac{\mathcal{T}_{12} \mathcal{T}_{2:m} e^{-2k_0 \text{Im}(n_2) d_2}}{1 - \mathcal{R}_{21} \mathcal{R}_{2:m} e^{-4k_0 \text{Im}(n_2) d_2}}, \quad (2.13)$$

$$\mathcal{R}_{1:m} = \mathcal{R}_{12} + \frac{\mathcal{T}_{12} \mathcal{R}_{2:m} \mathcal{T}_{21} e^{-4k_0 \text{Im}(n_2) d_2}}{1 - \mathcal{R}_{21} \mathcal{R}_{2:m} e^{-4k_0 \text{Im}(n_2) d_2}}, \quad (2.14)$$

where

$$\mathcal{R}_{ij} = \left| \frac{n_i - n_j}{n_i + n_j} \right|^2, \mathcal{T}_{ij} = \left| \frac{2n_i}{n_i + n_j} \right|^2. \quad (2.15)$$

A similar expression for a single etalon with $m = 3$ can be found in [24]. In our study, we have set $n_1 = n_m = n_{air} = 1$.

By assuming a specific form for the dielectric function of each layer, the parameters in the dielectric functions can be found by minimizing the sum of the squares of the errors between the theoretical transmittance of a multilayer structure and the experimental data. Specifically, the minimization problem can be written as

$$\min \sum_{i=1}^M [(y_{\parallel}(\omega_i) - \mathcal{T}_{1:m}(\omega_i; n_{1\parallel}, \dots, n_{m\parallel}))^2 + (y_{\perp}(\omega_i) - \mathcal{T}_{1:m}(\omega_i; n_{1\perp}, \dots, n_{m\perp}))^2], \quad (2.16)$$

where M is the total number of data points, $y_{\parallel}(\omega_i)$ and $y_{\perp}(\omega_i)$ are the locally averaged transmittance data at ω_i when the polarization of the incident light is parallel and perpendicular to the LC director, respectively. The two principal refractive indices of each layer are given by

$$n_{j\parallel} = \sqrt{\varepsilon_{j\parallel}(\varepsilon_{\infty\parallel}^j, \bar{A}_{\parallel}^j, \bar{\omega}_0^j, \bar{\sigma}^j)}, n_{j\perp} = \sqrt{\varepsilon_{j\perp}(\varepsilon_{\infty\perp}^j, \bar{A}_{\perp}^j, \bar{\omega}_0^j, \bar{\sigma}^j)}, j = 1, \dots, m, \quad (2.17)$$

and the dielectric functions $\varepsilon_{j\parallel}$ and $\varepsilon_{j\perp}$ are modeled either as a Sellmeier equation in Eq. (1.2), or as a causal Gaussian oscillator model in Eqs. (1.5)-(1.7), where $\varepsilon_{\infty\parallel}^j, \varepsilon_{\infty\perp}^j, \bar{A}_{\parallel}^j, \bar{A}_{\perp}^j, \bar{\omega}_0^j, \bar{\sigma}^j$ are the fitting parameters. The lengths of the vector parameters $\bar{A}_{\parallel}^j, \bar{A}_{\perp}^j, \bar{\omega}_0^j, \bar{\sigma}^j$ are equal to the number of oscillators. We have assumed that the peak locations $\bar{\omega}_0^j$ and their widths $\bar{\sigma}^j$ along the two principal directions are the same, but the amplitudes $\bar{A}_{\parallel}^j, \bar{A}_{\perp}^j$ are different, as suggested by the experimental data.

We note that one can't model all the layers collectively as an effective single layer, which disregards the arrangement of the layers, since, in general, the transmittance of the multilayer structure may sensitively depend on the order of the layers. It is also impossible to determine the refractive indices of all layers simultaneously from a single transmittance measurement of all layers, as the solutions won't be unique. Therefore, ideally, we should determine the dielectric response of each layer separately, but this is often not practically viable. However, we can measure, for example, the transmittance of a single glass layer first, and then that of a single glass layer coated with indium tin oxide (ITO) layer, and next that of a polyimide (PI) alignment layer on top of the glass and ITO layers. These three measurements enable us to determine the dielectric properties of glass, ITO, and PI iteratively, one at a time. To determine the dielectric properties of dye-LC mixtures, we assume the effect of a dye guest on the dielectric response of the mixture is an additive contribution to that of the pure LC host. With this in mind, we first use the transmittance spectrum of pure LC in the cell to determine the dielectric function of LC host, and then use the transmittance spectrum of dye-LC mixture in the cell to determine the contribution of dye to the dielectric function of dye-LC mixture.

We have implemented the Levenberg–Marquardt algorithm to solve the above minimization problems. It is important to note that the function to be minimized, Eq. (2.16), has multiple local minima. To obtain the most faithful fitting results, we have carefully selected the initial parameters which give a crude agreement of the experimental and model transmittances. Specifically, the absorption peak positions ω_{0k} were chosen to be in proximity of the dips of the transmittance spectra. The number of oscillators used in modeling each layer is determined by whether or not the addition of one more oscillator improves the fitting significantly. The goodness of fit is assessed from maximum pointwise errors, rather than an averaged error.

3 Experiment

Our liquid crystal cells typically use two glass substrates with each substrate coated with a conductive ITO layer enabling the application of an electric field across the cell. The PI alignment layer, next to the ITO layer, is buffed antiparallel on the two substrates to impose the homogeneous boundary conditions on the nematic directors. The thicknesses of the glass, ITO and PI layers are approximately 1mm, 100 nm and 100 nm respectively. The thickness of the cell gap is approximately $20\mu m$. The empty cells are filled with pure LCs or with dye-LC mixtures, with 1% or 0.5% dye concentrations.

As discussed in Section 2, we separately measured the transmittance spectra of the following samples: a single glass, glass with ITO layer, glass with ITO and PI layers, empty cell, pure LC in the cell, and dye-LC mixtures in the cell. To measure the transmittance spectra of each sample, we use a spectrometer with a

polarizer. The sample is aligned so that light is normal incident on the cell. The polarizer is oriented so that light is polarized parallel, as shown in Fig. 1(a), or perpendicular, in Fig. 1(b), to the nematic director.

The transmission spectra are measured using an Ocean Optics HR400CG-UV-NIR High-Resolution Spectrometer with resolution $\sim 0.2 - 0.3$ nm with an Ocean Insight DH-2000-BAL light source covering the range of 300 nm to 900 nm.

Since the resolution of the spectrometer is high and sample is thin, the transmittance shows some oscillations due to multiple reflections and interference. As it is preferable to work with a smooth spectra for fitting purposes, local averaging of the transmittance was carried out before the fitting procedure. Measurement errors were estimated by comparing repeated spectral measurements on single cells. Variations due to differences in cell properties were estimated by comparing the spectra of six empty cells. The combined variations gave an estimated uncertainty of approximately 5% in the wavelength range 300 to 900 nm.

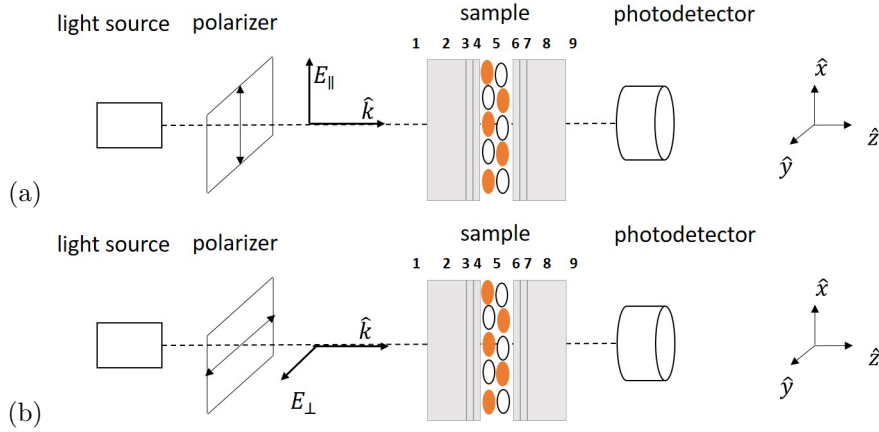


Figure 1: Schematic of the experimental setup. Light propagating in the \hat{z} -direction is normally incident on the cell. The LC director \hat{n} is in the \hat{x} -direction. The transmittance is measured when the polarization of the light is (a) parallel to the \hat{n} , and (b) perpendicular to \hat{n} . The sample between the polarizer and the photodetector represents the LC cell where a dye-LC mixture is contained in two glass(2,8) substrates coated with ITO (3,7) and PI (4,6) layers. Layers labeled 1 and 9 are air. The sample may also be a single glass, glass coated with ITO, glass coated with ITO and PI for separate measurements.

4 Results

In this section, we first characterize the dielectric function of each substrate layer using the causal Gaussian oscillator model for glass and the Sellmeier equation for ITO and PI in section 4.1. Knowing the refractive indices of substrate layers, we then proceed to characterize the dielectric function of the pure LC and two dye-doped liquid crystal mixtures in section 4.2.

4.1 Dielectric functions of the substrate layers

The transmittance spectra of the substrate layers: glass only, glass with ITO, and glass with ITO and PI, are shown in Fig. 2(a). The transmittance spectra of the three layers do not show significant polarization dependence, thus we regard all substrate layers as optically isotropic.

Our strategy is as follows: we start with the characterization of the dielectric function of glass with the transmittance spectrum of a single slab of glass. Next, we obtain the dielectric function of ITO by fitting the transmittance spectrum of glass with ITO, given we have already known the refractive index of glass. Lastly, the dielectric function of the PI is found by fitting the transmittance spectrum of glass with ITO and PI layers, given the dielectric functions of glass and ITO. The results are shown in detail below.

4.1.1 glass

Glass is generally taken to be transparent in the visible range. The dispersion relation was generally modeled with Sellmeier equation in [25, 26].

In this work, the dielectric function of glass is characterized solely based on the transmittance spectrum of a single glass slab in the range of 300 – 900 nm. In Eqs. (2.13)-(2.15), we set $m = 3, n_1 = n_3 = 1$, and solve the minimization problem Eq. (2.16) to find $n_2 = n_{glass}$. We first attempted to use the Sellmeier equation for ε_{glass} . Here, the one-term Sellmeier equation was fitted with parameters $\varepsilon_\infty = 1.5302, A = 0.6001, \omega_0 = 2\pi c/309.19nm$, and the predicted transmittance of the 3-layer structure is shown as the green dot-dashed curve in Fig. 2(b). We observed that the Sellmeier equation cannot accurately capture the sharp corner in the transmittance spectrum near 300 nm due to the nature of polynomial decay away from the absorption peak; it also fails to model the observed slow decrease of transmittance between about 600 and 900 nm. In addition, since the peak of the oscillator is located at 309 nm, the dielectric constant diverges near the peak, which is nonphysical.

We therefore used the causal Gaussian oscillator model for ε_{glass} . We have used two such oscillators, with one oscillator peak at 195 nm for the strong absorption in the near-UV and one at 987.31 nm for the slow decrease in the transmittance over visible to near-IR. The causal Gaussian oscillator model produces excellent agreement between the theoretical transmittance of the 3-layer structure and the experimental data as shown in Fig. 2(b). The average relative error in the range of 400 – 900 nm is 0.8%. The real and imaginary parts of the refractive indices of glass, calculated via the causal Gaussian oscillator model with parameters given in Table 1, are plotted in Fig. 3. The real part of the refractive index of the glass is about 1.53 – 1.54. A more sophisticated model combining Sellmeier and causal Gaussian can be used [27] to produce larger variation in the refractive indices with respect to wavelength. However additional information would be needed to decide which model is preferable, hence we do not pursue this topic in this work. The refractive index of the glass given by the causal Gaussian oscillator model is used for the subsequent characterizations of dielectric functions of the remaining layers of the LC cell.

4.1.2 ITO layer

For modeling of the dielectric function of the ITO, in the literature, either a combination of a single Drude oscillator for free carriers and double Lorentz oscillators for strong absorption in the near-UV [28], or a combined Drude, causal Gaussian oscillators and a Cauchy term [29] were used.

Here, the dielectric function of ITO is characterized based on the transmittance spectrum of glass coated with an ITO layer in the range of 300 – 900 nm. In Eqs. (2.13)-(2.15), we set $m = 4, n_1 = n_4 = 1$, and $n_2 = n_{glass}^{cG}$, which is obtained from the causal Gaussian oscillator model in Sec. 4.1.1. We then solve the minimization problem Eq. (2.16) to find $n_3 = n_{ITO}$. By comparing the transmittance of glass with ITO with that of glass with ITO and PI in Fig. 2(a), we observe that the transmittance of the 5-layer structure in the near-UV is higher than that of the 4-layer structure. Absorption in the near-UV from the ITO or from the PI won't be able to produce such a spectrum. This increase in the transmittance with more layers can only be explained by index matching. Therefore, we model the dielectric functions of both the ITO layer and PI layer with the Sellmeier equation. For the ITO, the Sellmeier equation with two peaks, one at 275.01 nm and the other at 1000.01 nm, produces excellent agreement between the theoretical prediction of transmittance of the 4-layer structure and the data, as shown in Fig. 2(c), with the average relative error 1% in the range of 400 – 900nm. Fig. 3(b) shows the refractive index of ITO calculated from the Sellmeier equation with parameters given in Table 1. In the range of 350 – 900 nm, the refractive index for ITO decreases from 2.2 to 1.6, which is consistent with that in the literature [30, 31].

4.1.3 PI layer

Buffered polyimide polymer layers can be optically anisotropic, with an average refractive index in the visible of about 1.5 – 1.8 depending on chemical structure and morphology [32, 33]. Our cells do not show appreciable birefringence, so we model the PI layer with a single principal dielectric function.

The dielectric function of PI is determined using the transmittance spectrum of glass with ITO and PI layers from 300 – 900 nm. In Eqs. (2.13)-(2.15), we set $m = 5, n_1 = n_5 = 1, n_2 = n_{glass}^{cG}$ obtained from Sec. 4.1.1 and $n_3 = n_{ITO}^S$ obtained from Sec. 4.1.2. We then solve the minimization problem Eq. (2.16) to

find $n_4 = n_{PI}$. As discussed in 4.1.3, we model the dielectric function of PI with the Sellmeier equation. A two-term Sellmeier equation is fitted with one peak located at 199.32 nm, and the other in the IR at 1135.22 nm. The corresponding theoretical transmittance of the 5-layer structure shows reasonable overall agreement with experimental data, with slightly larger discrepancy in the 300 – 500 nm region, as shown in Fig. 2(d). The average relative error in the range of 400 – 900nm is 1%. Surprisingly, the contribution of the PI layer to the transmittance varies dramatically from one piece of substrate to another. Therefore, we only aim to get a reasonable fitting here. Fig. 3(b) shows the refractive index of PI calculated from the Sellmeier equation with parameters given in Table 1. The refractive index of PI decreases from 1.95 to 1.54 in the 350 to 900 nm range, in agreement with reported values in [34, 35, 36].

We note that the fitting parameters of the Sellmeier equations for the ITO and PI layers are independent of the thicknesses of the ITO and PI layers, since we have considered the averaged transmittance which depends on the values of the (real) refractive indices but not on the cell thickness.

The goodness of fit for the dielectric functions of the three substrate layers was further tested by comparing the experimental measurements of empty cells with the theoretical prediction of the transmittance of the 9-layer structure with $m = 9, n_1 = n_5 = n_9 = 1, n_2 = n_8 = n_{glass}^C, n_3 = n_7 = n_{ITO}^S, n_4 = n_6 = n_{PI}^S$, using fitted model parameters in Table 1. The experimental data is plotted as the average over the measurements of six different empty cells, with upper and lower bounds from the six measurements at each wavelength. Our theoretical prediction of the empty cell shows reasonable agreement with these measurements, with a larger discrepancy near 300 – 500 nm as shown in Fig. 4. This is mainly due to the imperfection of the PI fitting at near-UV. We note that since the fitting for the PI didn't show excellent agreement between theory and measurement in the near-UV, the error in the PI fitting will carry over to the fitting of the LC and subsequent dye-LC mixtures. Even though the relative error in the near-UV made in the previous steps carried forward, it is not significant enough to invalidate the subsequent steps. If a highly accurate characterization in the near-UV is needed, more accurate measurements will also be required.

	ε_∞		A_k	ω_{0k}	σ_k (THz)
Glass(Gaussian)	2.3104	$k = 1$	0.2107	$2\pi c/195.02nm$	34851
		$k = 2$	0.00001	$2\pi c/987.31nm$	3127
ITO(Sellmeier)	1.1221	$k = 1$	1.4299	$2\pi c/275.01nm$	—
		$k = 2$	0.0641	$2\pi c/1000.01nm$	—
PI (Sellmeier)	2.4779	$k = 1$	0.7831	$2\pi c/199.32nm$	—
		$k = 2$	0.5697	$2\pi c/1315.22nm$	—

Table 1: Fitted parameters in the dielectric functions of glass, ITO and PI. Here c is the speed of light in air.

4.2 Dielectric functions of dye-doped liquid crystal mixtures

Liquid crystals are typically birefringent, as are oriented dichroic dyes. When the transmittance of a mixture is measured with the polarization of incident light either parallel or perpendicular to the LC director, only one principal refractive index contributes to the transmittance. The alignment of LCs and dye mixtures was confirmed by applying a voltage across the cell. Since the LC has a negative dielectric anisotropy at low frequency, no change in orientation is expected, and none was observed.

We assume that dielectric functions of the LC and of the dye can be treated as additive. This is valid when the mixture is homogeneous and the concentration of dye is low. The experimental data suggest that the locations of the absorption peaks and their broadenings are nearly the same for both polarizations and only the magnitudes differ. The two principal dielectric functions of dye-doped LC mixtures are then given

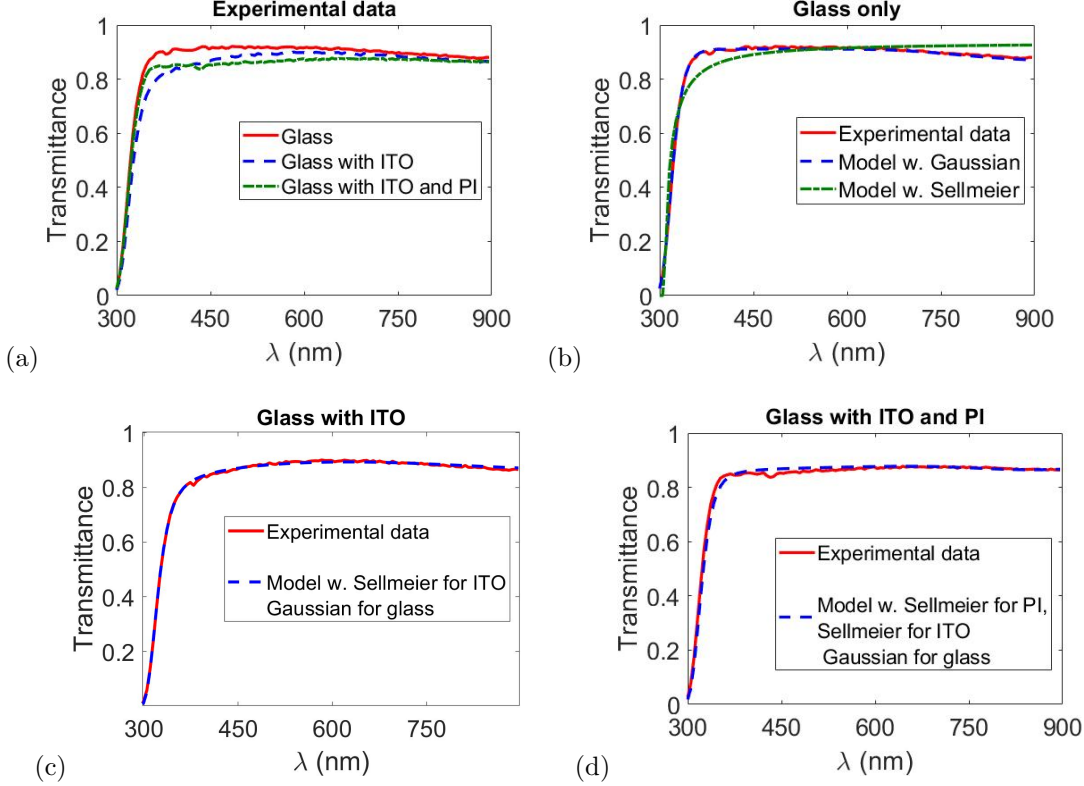


Figure 2: Transmittance of substrate layers. (a) shows the averaged experimental transmittance spectra of glass only, glass with ITO, and glass with ITO and PI. (b, c, d) show the averaged experimental data and theoretical prediction of multilayer structures using dielectric functions of substrate layers with fitting parameters in Table 1, for glass only, glass coated with ITO, and glass coated with ITO and PI, respectively.

as

$$\varepsilon_{\parallel}^{LC+dye} = \varepsilon_{\infty\parallel}^{LC} + \sum_{k=1}^2 \chi_k^S(\omega; A_{k\parallel}^{LC}, \omega_{0k}^{LC}) + c_{dye} \sum_{k=1}^{N_{dye}} \chi_k^{cG}(\omega; A_{k\parallel}^{dye}, \omega_{0k}^{dye}, \sigma_k^{dye}), \quad (4.1)$$

$$\varepsilon_{\perp}^{LC+dye} = \varepsilon_{\infty\perp}^{LC} + \sum_{k=1}^2 \chi_k^S(\omega; A_{k\perp}^{LC}, \omega_{0k}^{LC}) + c_{dye} \sum_{k=1}^{N_{dye}} \chi_k^{cG}(\omega; A_{k\perp}^{dye}, \omega_{0k}^{dye}, \sigma_k^{dye}), \quad (4.2)$$

where c_{dye} denotes the concentration of the dye, and N_{dye} the number of oscillators associated with the dye. The first sum accounts for the contribution from the LC host and the second from the dye guest. In Eqs. (2.14)-(2.13), we set $m = 9$, $n_1 = n_9 = 1$, $n_2 = n_8 = n_{glass}^{cG}$, $n_3 = n_7 = n_{ITO}^S$, $n_4 = n_6 = n_{PI}^S$, and try to find n_5 which minimizes the sum of squared errors of the model and data. In what follows, we first obtain the pure LC contribution of the first two terms before the dye is introduced.

4.2.1 liquid crystal host

The ordinary refractive index n_o of the LC typically ranges from 1.50 – 1.57 while extraordinary refractive index n_e can range from 1.5 – 1.9 depending on molecular structure, temperature and wavelength [37]. Many models, Cauchy or Sellmeier, have been proposed to model the wavelength and temperature dependence of the refractive indices of LCs [38, 39, 40].

In this work, the characterization of the dielectric function of the LC host is based on the transmittance spectra of the cell containing pure LC host from 300 – 900 nm. The LC appears to be transparent at visible

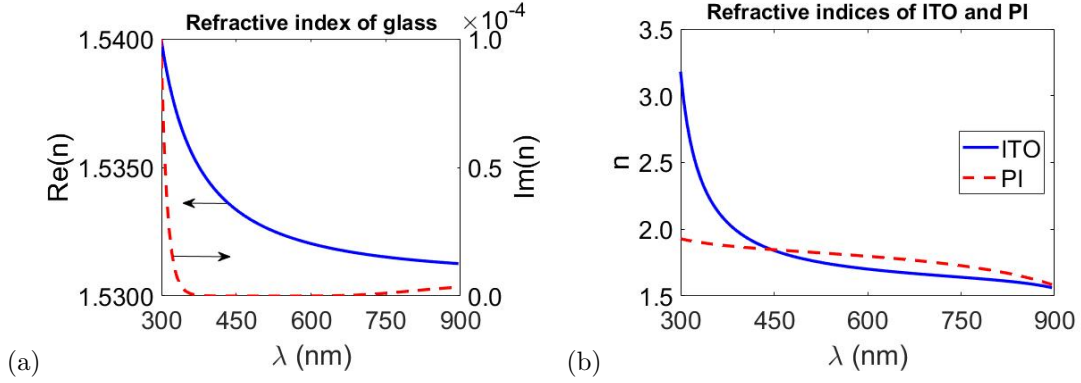


Figure 3: (a) Refractive index of the glass substrate. (b) Refractive indices of the ITO and PI layers.

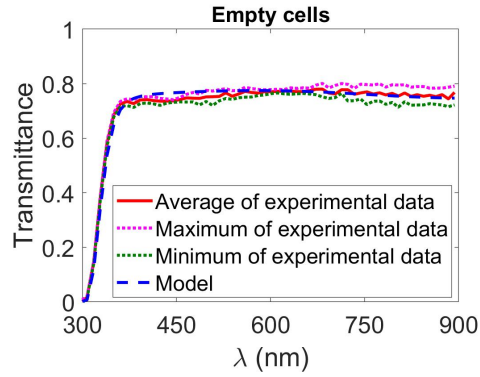


Figure 4: Average of measured transmittance spectra of six empty cells together calculated values using dielectric functions of substrate layers with fitted parameters in Table 1. The solid red curve is the measured transmittance averaged over six cells, bounded by the upper and lower extreme values (dotted curves) among the six measurements at each wavelength.

wavelengths, but with appreciable reduction of the transmittance in the near-UV. In order to understand the origin of this reduction, we carried out a further set of experiments, where three pure LC cells with the same glass substrates but with different thicknesses, $5\mu\text{m}$, $20\mu\text{m}$, $47\mu\text{m}$, were prepared and transmittance spectra were measured. The results show that the transmittances of the LC cells are apparently independent of gap thickness, which implies that the LC host is nonabsorptive. This prompts us to use the Sellmeier equation for the dielectric function of LC host. A two-term Sellmeier equation with one peak located at 125.01 nm and the other at 289.62 nm was obtained from the fit. Fig. 5(a) shows reasonable agreement between the theoretical predictions and experimental measurements for both polarizations; it is expanded in the visible range in Fig. 5(b) to allow better visual assessment. The average relative error is about 1% in the range of 400 – 900 nm. The larger discrepancy of fitting and data occurs at short wavelengths in the near-UV, where larger experimental measurement errors likely occur. Figure 6 shows the two principal refractive indices of the host LC calculated with Sellmeier with parameters given in Table 2. Our LC host is a multicomponent mixture, with manufacturer provided refractive indices $n_e = 1.55$ and $n_o = 1.47$ without any wavelength dependence information. Our results show reasonable agreement with the manufacture's data.

4.2.2 dichroic dye and liquid crystal mixtures

Lastly, we report the characterization of the dielectric functions of two dye-LC guest-host mixtures. The concentration of dye in the dye-LC mixture is approximately 1%. The dielectric functions of the dye-LC mixtures are modeled as Eqs. (4.1) -(4.2). The first two terms in both equations have already been acquired in Sect. 4.2.1; here we only need to obtain the last term which only contains the dye contribution.

The first dye, referred to as dye 1032, is orange in color. We have used four causal Gaussian oscillators for the contribution of this dye. One is peaked at 304.07 nm for the slight absorption near 300 nm, and two are at 455.08 and 495.89 nm for the strong absorption near 465 nm, and one at 683.51 nm for slight absorption at longer wavelength. We note that a single oscillator near the 465 nm is not sufficient to accurately fit both the breadth and shape of the transmittance spectrum. The second dye, referred to as dye 4102, is blue in color. The transmittance spectrum clearly shows two peaks between 600 – 750 nm, as shown in Fig. 7(b). We have tried to use three causal Gaussian oscillators with one in the near-UV and two in the visible, but these can't reproduce the shape of transmittance spectrum near 600 nm. We have then used four causal Gaussian oscillators, one is peaked at 291.23 nm for the absorption in the near-UV, and three in the visible at 594.28, 645.31 and 688.63 nm, respectively. The fit results for LC mixture with dyes 1032 and 4102 are shown in Fig. 7(a) and (b), respectively, showing excellent agreement of the experimental measurements and theoretical predictions. The average relative errors are 2% in the range of 400-900 nm. Figure 8 shows the corresponding refractive indices of dye-LC mixtures calculated from the combined Sellmeier and causal Gaussian oscillator models with parameters given in Table 2. Both dyes show only weak absorption for perpendicular polarization in the visible; the values of $A_{\perp k}$ are much smaller than those of $A_{\parallel k}$. This is an indication of a good alignment of dye molecules with the nematic director.

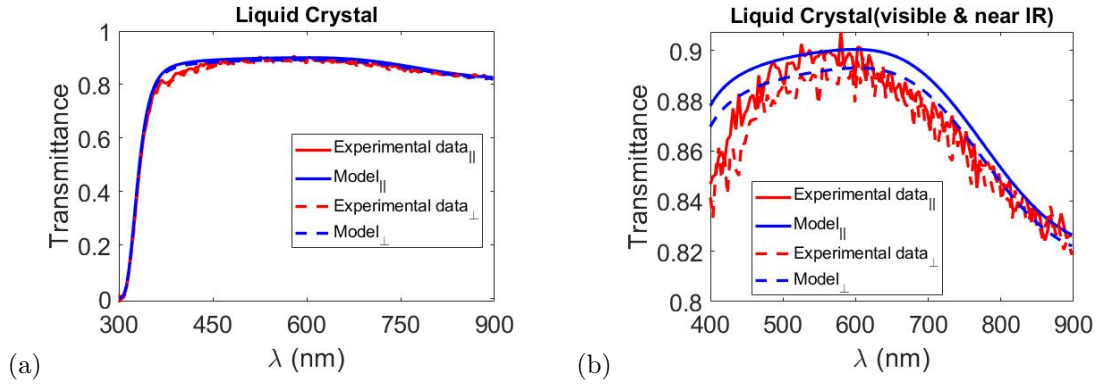


Figure 5: (a) Transmittance spectra of an LC sample without dye in a cell. (b) Expanded region of (a) in the visible region. Solid red curves show experimental results, and dashed blue curves indicate predictions from model with two Sellmeier oscillators for ϵ_{LC}^S with fitted parameters in Table 2.

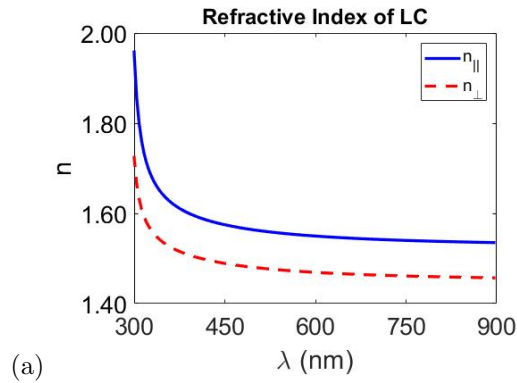


Figure 6: Refractive indices of nematic LC for polarization (a) parallel and perpendicular to the LC director.

To test the usefulness of our model, we examine the goodness of the theoretical prediction of 0.5% dye concentration in LC. We set $c_{dye} = 0.5\%$ in Eqs. (4.1)–(4.2) and keep all the other parameters the same to obtain the dielectric functions of 0.5% dye-LC mixtures via Eqs. (4.1)–(4.2). We then use Eq. (2.13) with $m = 9$ to calculate the transmittance spectra of the cell. The results are given in Fig. 9, showing excellent agreement with experimental measurements 0.5% dye in LC, with average relative errors 3% in the range of

	$\varepsilon_{\infty\parallel} = 1.1649$	$\varepsilon_{\infty\perp} = 1.0149$		
liquid crystal	$A_{\parallel k}$	$A_{\perp k}$	ω_{0k}	σ_k (THz)
$k = 1$	1.0671	1.0341	$2\pi c/125.01nm$	—
$k = 2$	0.0932	0.0482	$2\pi c/289.62nm$	—
dye 1032				
$k = 1$	0.5211	0.2701	$2\pi c/304.07nm$	12896
$k = 2$	0.5098	0.0001	$2\pi c/455.08nm$	16593
$k = 3$	0.3207	0.0210	$2\pi c/495.89nm$	25654
$k = 4$	0.0191	0.0298	$2\pi c/683.51nm$	7236
dye 4102				
$k = 1$	0.4001	0.3799	$2\pi c/291.23nm$	15375
$k = 2$	0.2234	0.0288	$2\pi c/594.28nm$	12708
$k = 3$	0.5089	0.0794	$2\pi c/645.31nm$	18050
$k = 4$	0.4119	0.0686	$2\pi c/688.63nm$	40319

Table 2: Fitted parameters in the combined Sellmeier and causal Gaussian oscillator model with contributions from liquid crystal, dye 1032 and dye 4102. Here c is the speed of light in air.

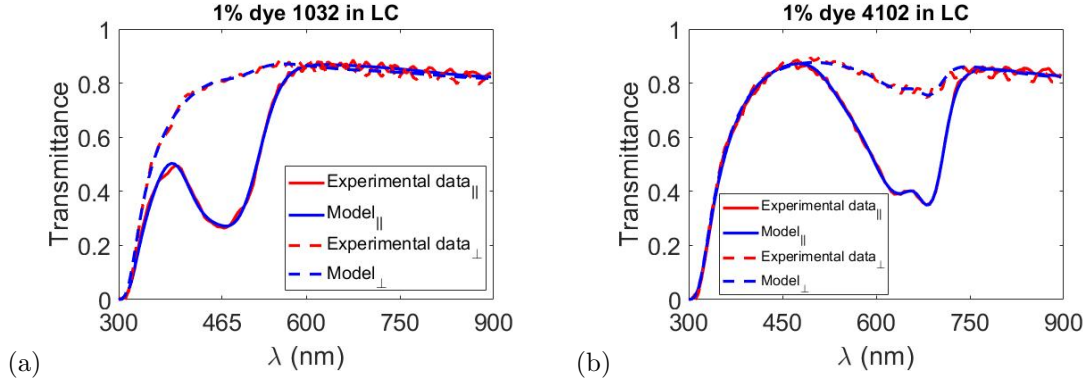


Figure 7: Transmittance spectra of mixture (a) 1% dye 1032 in LC and (b) 1% dye 4102 in LC. Solid red curves are experimental data, and dashed blue curves are calculated transmittance of structures using the combined Sellmeier and causal Gaussian oscillator model for ε_{LC+dye} with fitted parameters in Table 2.

400-900 nm. We are confident to conclude that the dye and liquid crystal mixtures we have studied behave linearly, which makes the modeling straightforward and we can effectively predict the transmittance at any concentration of dye-LC mixture, in the low concentration regime.

In Ref. [18], the assumed dielectric function has uncorrelated real and imaginary parts. This allows the use of the Beer-Lambert law to obtain the extinction coefficients in a simple way, disregarding their dependence on the substrate layers. Our method, however, deals with the more general case when the real and imaginary parts cannot be assumed to be independent and multiple reflections are properly considered in all the layers.

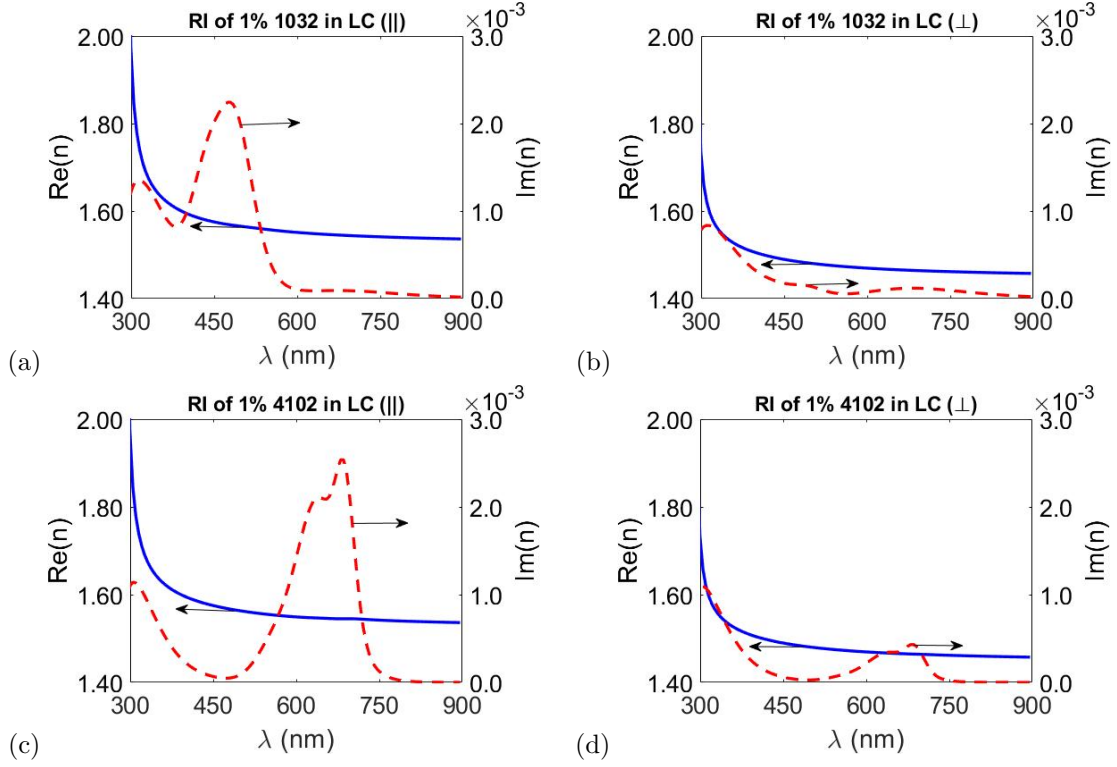


Figure 8: Top: Refractive indices of 1% dye 1032 in LC. Bottom: Refractive indices of 1% dye 4102 in LC. Left: principle refractive indices for polarization along the LC director; Right: principle refractive indices for polarization perpendicular to LC director.

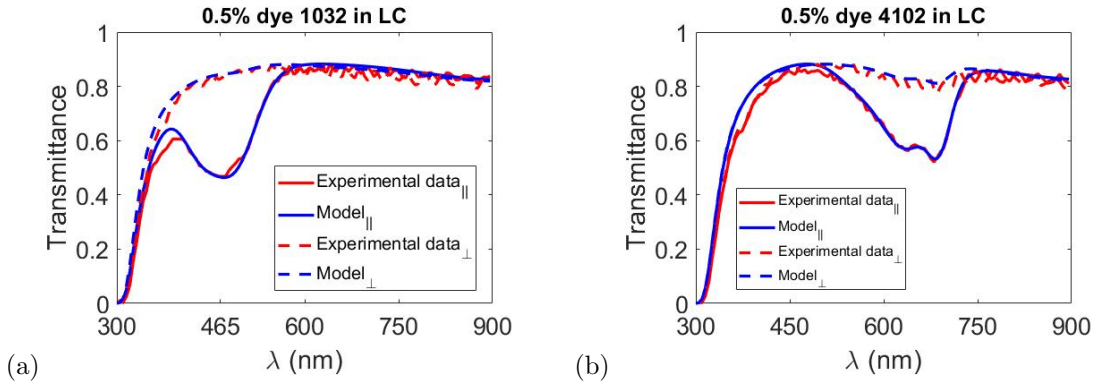


Figure 9: Transmittance spectra of 0.5% dye (a) 1032 and (b) 4102 in LC. Solid red curves are experimental data, and dashed blue curves are calculated values using the combined Sellmeier and causal Gaussian oscillator model for ϵ_{dye+LC} with fitted parameters in Table 2 and scaled amplitudes.

5 Conclusions

In this work, we have characterized the wavelength dependence of the refractive indices of dichroic dye-liquid crystal guest-host systems from the near-UV/vis (300 to 900 nm) transmittance spectra. The dye-LC mixtures are contained in planar cells, where the substrates are glass coated with ITO and PI layers. The PI layer is buffed in the plane to impose in-plane orientation of the LC director, which in turn aligns the dichroic dye in the same direction. When linearly polarized light parallel or perpendicular to the LC director is normally incident on the sample, only one principal refractive index of the dye-LC system contributes to the transmittance of the sample. These experimental arrangements allow characterization of the two principal components of a uniaxial material independently.

We have used the Sellmeier equation for the dielectric functions of the transparent layers away from their absorption peaks, and the causal Gaussian oscillator model for layers showing appreciable absorption in the near-UV/vis. Both models satisfy the Kramers-Kronig causality relations. The parameters in the dielectric function of each layer were obtained by minimizing the sum of squared errors between theoretical predictions and measurements of the transmittance.

Experimental measurements on substrate layers show no polarization dependence, hence all substrate layers are modeled as optically isotropic. The dielectric function of glass is modeled by the causal Gaussian oscillators with one peak in the near-UV for the strong absorption around 300 nm and one in the near IR for the slight decrease in the transmittance at long wavelengths. The dielectric functions of the ITO and PI layers are modeled by Sellmeier model with two oscillators: one near-UV and one near-IR.

To model the two principal dielectric functions of the dye-LC mixtures, we have used the combined Sellmeier and causal Gaussian oscillator models. We assume that each oscillator has the same resonance location and width, but different amplitudes, in the two principal directions, as indicated by the experimental data. The dielectric function of the liquid crystal host was characterized first, before introduction of the dye. The dielectric function of the pure LC host is modelled by the Sellmeier equations with two near-UV oscillators. The dye contribution to the dielectric function of dye-LC mixtures is modeled by the addition of causal Gaussian oscillators. For the two dye-LC mixtures reported, we have used four oscillators for each dye. Each dye contains one oscillator in the near-UV, and the others are placed at visible wavelengths to account for the absorption.

The causal Gaussian oscillator model can accurately characterize the dielectric function of dichroic dyes in liquid crystals in the near-UV/vis range in the low concentration regime. We have also used the same approach to model commercial dyes in isotropic solvents and obtained similar excellent quantitative agreement between theory and experiment.

Knowing the dielectric functions of dichroic dyes in LCs allows further analysis of different variation of the guest-host LC devices. Based on our results we expect to be able to predict the transmittance and reflectance of samples with inhomogeneous director fields, with different dye concentration and arbitrary angles of incidence in similar multilayer structures. The transmittance spectrum of the sample can be mapped onto the colors perceived by the human eye, leading, ultimately to the optimal design of LC devices.

Acknowledgments

The dye-mixtures are provided by AlphaMicron Inc. This work was supported by Air Force contract FA8649-20-C-0011 as part of the STTR AF18B-T003 Electronically Dimmable Eye Protection Devices (EDEPD) program and by the Office of Naval Research through the MURI on Photomechanical Material Systems (ONR N00014-18-1-2624).

Conflicts of interest

There are no conflicts of interest to declare.

References

- [1] Heilmeyer GH, Zanoni LA. Guest-host interactions in nematic liquid crystals. a new electro-optic effect. *Appl Phys Lett*. 1968;13(3):91-92.
- [2] Cox RJ. Liquid crystal guest-host systems. *Mol Cryst Liq Cryst*. 1979;55(1):1-32.
- [3] Scheffer TJ. Guest-host devices using anisotropic dyes. *Phil Trans R Soc Lond*. 1983;309(1507):189-201.
- [4] Sims MT. Dyes as guests in ordered systems: current understanding and future directions. *Liq Cryst*. 2016;43(13-15):2363-2374.
- [5] Incoe MN, Gould JH, Corning ME, et al. Relation between the absorption spectra and the chemical constitution of Dyes: XXIX. Interaction of direct azo dyes in aqueous solution. *J Res Nat Bur Stand*. 1958;60:65-83.
- [6] Hilfiker JN, Tiwald T. Dielectric function modeling. *Spectrosc ELL PV* 2019; 212:115-153.
- [7] Born M. *Optik:Ein Lehrbuch der Elektromagnetischen Lichttheorie*. Berlin(DE): Springer; 1933.
- [8] Taqatqa O, Al AH. Spectroscopic ellipsometry investigation of azo dye and azo dye doped polymer. *EPJ AP*. 2006;37(1):61-64.
- [9] Andam N, Refki S, Ishitobi H, et al. Optical Characterization of Ultra-Thin Films of Azo-Dye-Doped Polymers Using Ellipsometry and Surface Plasmon Resonance Spectroscopy. *Photonics*. 2021;8(2):41.
- [10] Djorovic A, Meyer M, Darby BL et al. Accurate modeling of the polarizability of dyes for electromagnetic calculations. *ACS omega*. 2017;2(5):1804-1811.
- [11] Brendel R, Bormann D. An infrared dielectric function model for amorphous solids. *J Appl Phys*. 1992;71(1):1-6.
- [12] Ni W, Ambjornsson T, Apell SP, et al. Observing Plasmonic Molecular Resonance Coupling on Single Gold Nanorods. *Nano Lett*. 2010;10(1):77-84.
- [13] Darby BL, Auguie B, Meyer M, et al. Modified optical absorption of molecules on metallic nanoparticles at sub-monolayer coverage. *Nat Photonics*. 2016;10(1):40-45.
- [14] Orosco J, Coimbra CF. Optical response of thin amorphous films to infrared radiation. *Phys Rev B*. 2018;97(9):094301.
- [15] Meneses DD, Malki M, Echegut P. Structure and lattice dynamics of binary lead silicate glasses investigated by infrared spectroscopy. *Journal of non-crystalline solids*. *J Non Cryst Solids*. 2006;352(8):769-776.
- [16] Kitamura R, Pilon L, Jonasz M. Optical constants of silica glass from extreme ultraviolet to far infrared at near room temperature. *Appl Opt*. 2007;46(33):8118-8133.
- [17] Huang Y, Pandraud G, Sarro PM. Characterization of low temperature deposited atomic layer deposition TiO₂ for MEMS applications. *J Vac Sci Technol A*. 2013;31(1):01A148.
- [18] Goda K, Nagasawa M, Kimura M, Akahane T. Evaluation technique of cell thickness, pretilt angle, and twist angle for guest?host liquid crystal displays. *JOSA A*. 2013;30(4):717-25.
- [19] Sims MT, Abbott LC, Cowling SJ, et al. Dyes in liquid crystals: experimental and computational studies of a guest-host system based on a combined DFT and MD approach. *Eur J Chem*. 2015;21(28):10123-10130.
- [20] Fegan SK, Kirsch P, Müller-Plathe F. The alignment of dichroic dyes in a nematic liquid crystal: a molecular dynamics investigation. *Liq Cryst*. 2018;45(9):1377-1384.

- [21] Dineiro JM, Berrogui M, Alfonso S, et al. Complex unitary vectors for the direction of propagation and for the polarization of electromagnetic waves in uniaxial and absorbing dielectric media. *J Opt Soc Am A*. 2007;24(6):1767-1775.
- [22] Orfanidis SJ. *Electromagnetic waves and antennas*. New Jersey(US) Sophocles J. Orfanidis; 2016.
- [23] Jovanovic N, Papousek W. A 2x2 matrix algebra for electromagnetic wave propagation in stratified biaxial media. *Int J Electron Commun*. 2001;55(2):123-126.
- [24] Stenzel O. *The physics of thin film optical spectra: An Introduction* Berlin(DE): Springer; 2016.
- [25] Tatian B. Fitting refractive-index data with the Sellmeier dispersion formula. *Appl Opt*. 1984;23(24):4477-4485.
- [26] Ghosh G. Sellmeier coefficients and dispersion of thermo-optic coefficients for some optical glasses. *Appl Opt*, 1997;36(7):1540-1546.
- [27] Cushman CV, Sturgell BA, Martin AC, et al. Eagle XG® glass, optical constants from 230 to 1690 nm (0.73-5.39 eV) by spectroscopic ellipsometry. *Surf Sci Spectra*, 2016;23(1):55-60.
- [28] Losurdo M, Giangregorio M, Capezzuto P, et al. Parametrization of optical properties of indium-tin-oxide thin films by spectroscopic ellipsometry: Substrate interfacial reactivity. *J Vac Sci Technol A*. 2002;20(1):37-42.
- [29] Cleary JW, Smith EM, Leedy KD et al. Optical and electrical properties of ultra-thin indium tin oxide nanofilms on silicon for infrared photonics. *Opt Mater Express*. 2018;8(5):1231-1245.
- [30] Konig TA, Ledin PA, Kerszulis J, et al. Electrically tunable plasmonic behavior of nanocube polymer nanomaterials induced by a redox-active electrochromic polymer. *ACS Nano*, 2014;8(6):6182-6192.
- [31] Pan D, Feixue C, Junhua L et al. The Property of ITO Produced by Optical Thin Film Coating for Solar Cell. *Proceedings of 2020 IEEE 5th International Conference on Integrated Circuits and Microsystems (ICICM)*. 2020 Oct. 23-25; Nanjing, CH. IEEE;2020
- [32] Yang F, Zorinants G, Ruan L, et al. Optical anisotropy and liquid crystal alignment properties of rubbed polyimide layers. *Liq Cryst*. 2007;34(12):1433-1441.
- [33] Macdonald BF, Zheng W, Cole RJ. Reflection anisotropy spectroscopy: A probe of rubbed polyimide liquid crystal alignment layers. *Int J Appl Phys*. 2003;93(8):4442-4446.
- [34] French RH, Rodriguez-Parada JM, Yang MK, et al. Optical properties of materials for concentrator photovoltaic systems. *Proceedings of 2009 34th IEEE Photovoltaic Specialists Conference(PVSC)*. 2009 Jun 7-12; Philadelphia, US. IEEE.
- [35] Kumar V, Goyal PK, Gupta R, et al. Tailoring of optical band gap and refractive index of heat treated Kapton-H Polyimide. *Adv Appl Sci Res*. 2011;2(2):79-85.
- [36] Huang TT, Tsai CL, Tateyama S, et al. Highly transparent and flexible bio-based polyimide/TiO₂ and ZrO₂ hybrid films with tunable refractive index, Abbe number, and memory properties. *Nanoscale*, 8(25), 12793-12802.
- [37] Li J, Wen CH, Gauza S, et al. Refractive indices of liquid crystals for display applications. *JDT*, 2005;1(1):51.
- [38] Li J, Wu ST. Extended Cauchy equations for the refractive indices of liquid crystals. *Int J Appl Phys*. 2004. 95(3):896-901.
- [39] Abdulhalim I, Dispersion relations for the refractive indices and the effective birefringence of liquid crystals. *Mol Cryst Liq Cryst*. 1991;197(1):103-108.
- [40] Wu ST. A semiempirical model for liquid crystal refractive index dispersions. *Int J Appl Phys*. 1991;69(4):2080-2087.